Supplementary Information

Enthalpy-Uphill Exciton Dissociation at Organic/2D Heterostructures Promotes Free Carrier Generation

Fatimah Rudayni,[1,2] Kushal Rijal,[1] Neno Fuller,[1] Wai-Lun Chan[1,*]

1. Department of Physics and Astronomy, University of Kansas, Lawrence, Kansas 66045, US

2. Department of Physics, Jazan University, Jazan 45142, Saudi Arabia
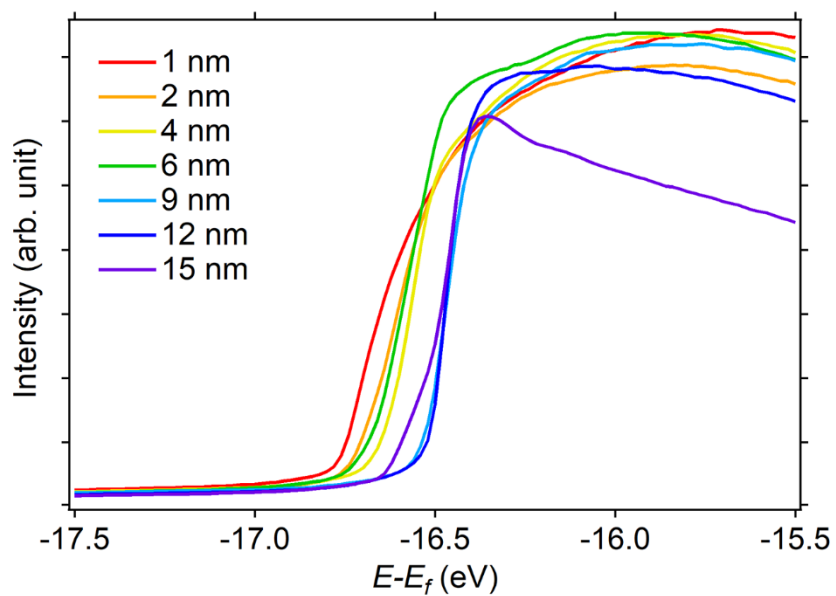
* wlchan@ku.edu

Fig. S1: The UPS spectra for F_8ZnPc films with different thicknesses grown on ML-WS_2. The energy window near the secondary electron cutoff (SECO) is shown. For thicknesses < 10 nm, the position of the SECO shifts to the right as the film thickness increases, which indicates an increase in the work function.
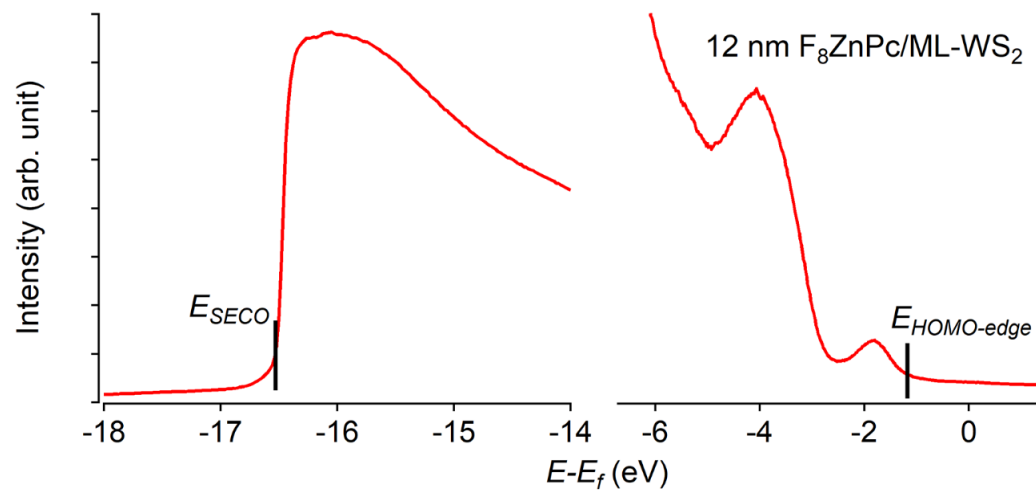
Fig. S2: A UPS spectrum for the 12-nm F_8ZnPc/ML-WS_2 sample. The positions of the SECO (E_{SECO}) and the rising edge of the HOMO peak ($E_{HOMO\text{-}edge}$) are indicated on the spectrum.

The ionization potential (IP) of the F_8ZnPc film is determined by:

$$IP = h\nu - (E_{HOMO-edge} - E_{SECO}),$$

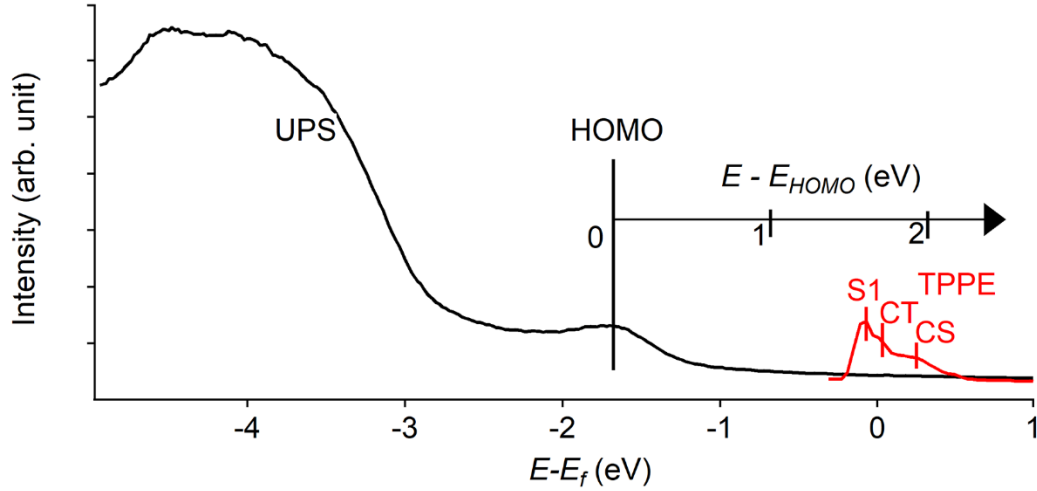where hυ is the photon energy. For the UPS measurement, hυ = 21.22 eV.

Fig. S3: The UPS spectrum (black) and TPPE spectrum at $t \sim 100$ ps (red) for the 1-nm F$_8$ZnPc/ML-WS$_2$ sample. We note that the UPS spectrum is plotted as a function of the initial state energy, while the TPPE spectrum is plotted as a function of the intermediate state energy.

In the main text, the energy of the TPPE spectrum is referenced with respect to the F$_8$ZnPc's HOMO peak energy (the E-E_{HOMO} axis in Fig. S3). During the TPPE measurement, excited electrons at the F$_8$ZnPc's LUMO are ionized by probe photons. Hence, the location of peaks in the TPPE spectrum, plotted as a function of E-E_{HOMO}, should correspond to the quasiparticle band gap ($E_{LUMO} - E_{HOMO}$) of the F$_8$ZnPc. However, the electron at the F$_8$ZnPc's LUMO can be bound with a hole in the F$_8$ZnPc (in the case of S$_1$ exciton), or a hole in the WS$_2$ (in the case of a CT exciton). In order to ionize these electrons, additional energy needs to be consumed to overcome the exciton binding energy (E_{ex-b}), which reduces the kinetic energy of the photoemitted electron. Therefore, the actual position of the peak should correspond to ($E_{LUMO} - E_{HOMO}$) - E_{ex-b}. In the case of the S$_1$ peak, the peak position represents the S$_1$ exciton energy.

The accuracy of the exciton energy determined by this method would be affected by different sample charging conditions induced by the different light sources used in the UPS and TPPE experiment, which can result in a relative energy shift between the two spectra. In order to improve the accuracy of the energy alignment between the UPS and TPPE spectra, we first plot the two spectra as a function of the kinetic energy, and apply an energy offset to the TPPE spectra so that the SECO of the raw TPPE spectrum (background + pump induced signal) aligns with that of the UPS spectrum. The SECO should remain at the same position if there is no sample charging. In some samples, this correction can be around ~ 0.1 eV.
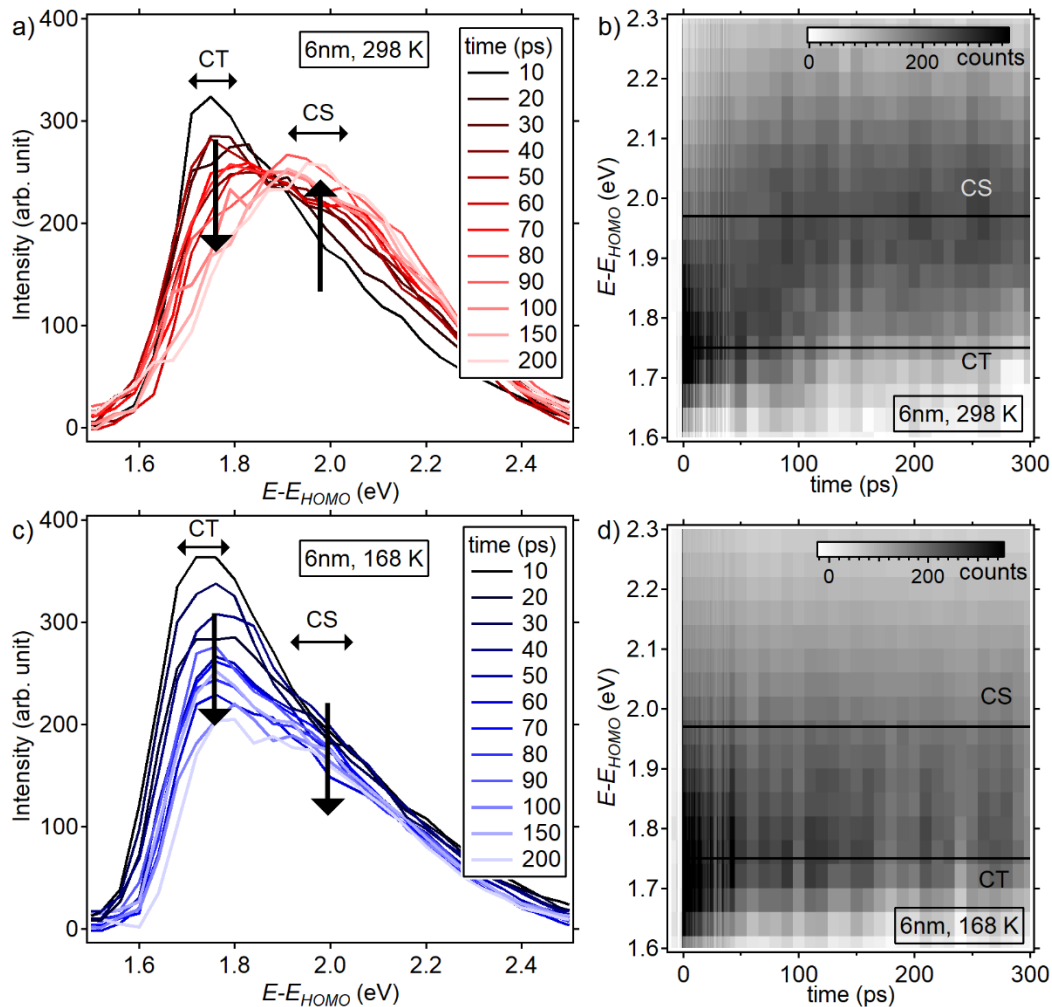
Fig. S4: (a) The raw spectra at different delay times for the 6-nm $F_8ZnPc/ML-WS_2$ sample collected at the room temperature. The black arrows on the plot show how the intensity evolves with time around the CT and CS states. (b) The 2D spectrum of the same sample collected at the room temperature plotted using a grayscale. (c) and (d) are same as (a) and (b) except that the spectrum is collected at 168 K.
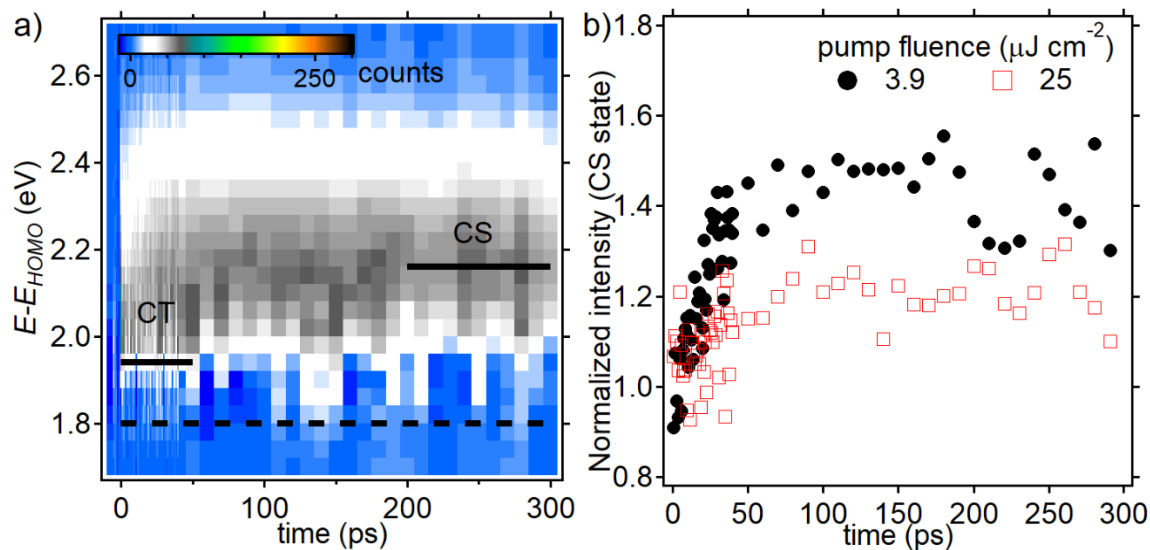
Fig. S5: (a) The TR-TPPE spectrum of the 6-nm $F_8ZnPc/ML-WS_2$ sample collected at a lower incident pump fluence (6.1 $\mu J\ cm^{-2}$ compared to 39 $\mu J\ cm^{-2}$ used for collecting the spectrum shown in Fig. 2 in the main text). (b) The normalized intensity of the CS state. The intensity is normalized by the intensity at early delay times (< 5 ps). The CS state is produced even at the lower pump fluence. Indeed, the charge generation yield is even larger at the lower fluence as indicated by the larger rise in the normalized signal.
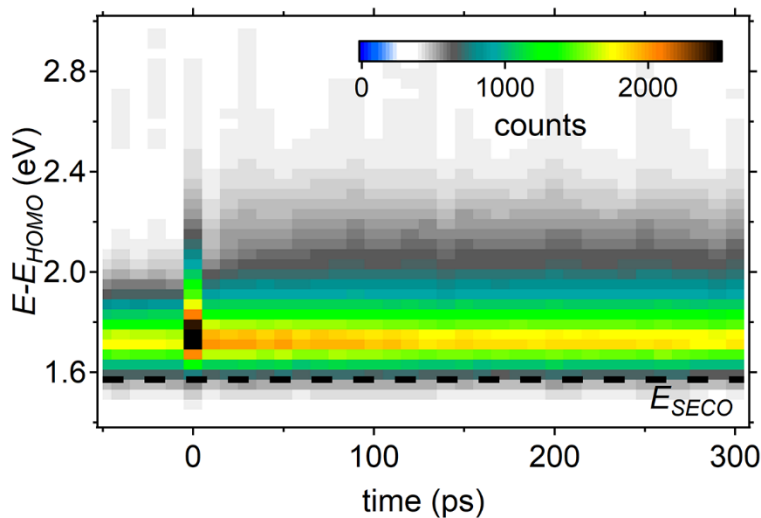

Fig. S6: (a) The raw TPPE spectrum (before subtracting the photoemission background at negative delay times) for the data shown in Fig. 2b in the main text. There is no observable shift in the SECO energy as a function of time. Hence, the energy upshift observed in Fig. 2b is not due to a transient change in the sample work function.
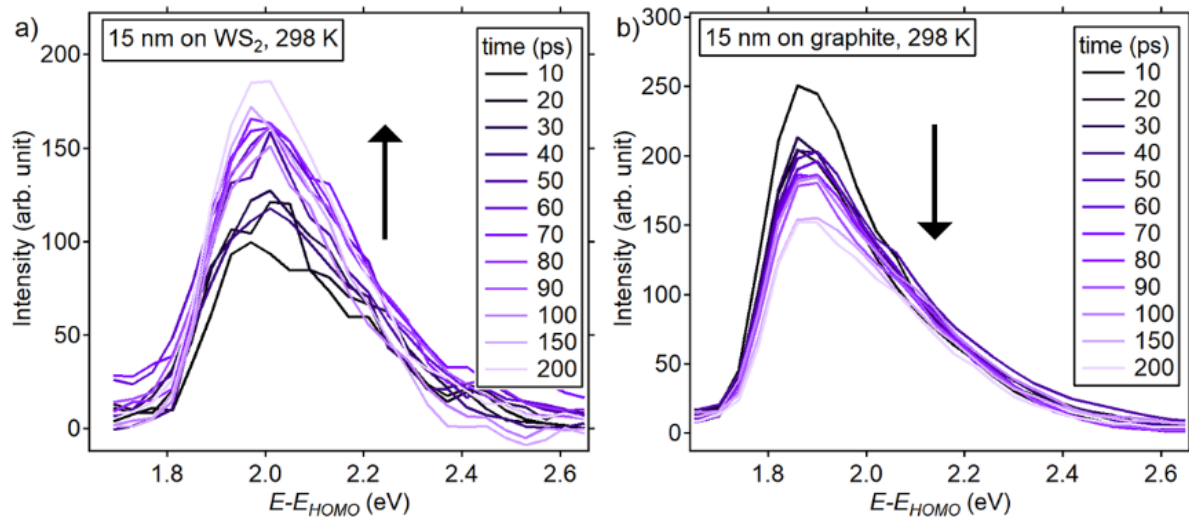
Fig. S7: (a) The raw spectra at different delay times for the 15-nm F_8ZnPc/ML-WS_2 sample collected at the room temperature. The black arrow on the plot shows how intensity evolves with time. (b) Same as (a), but for the 15-nm F_8ZnPc/graphite sample.
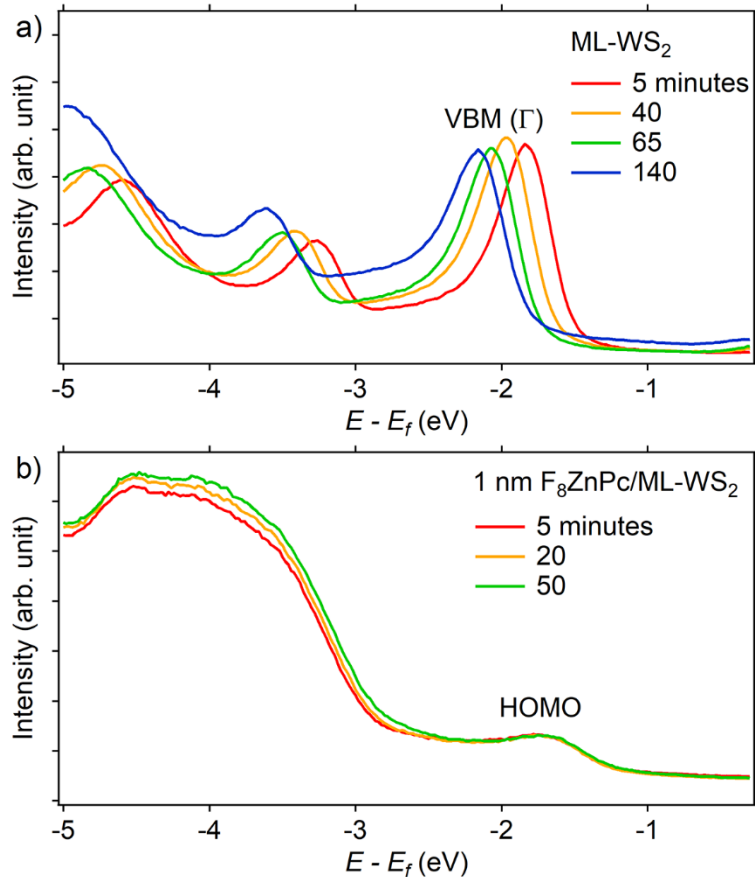
Fig. S8: UPS spectra for (a) ML-WS$_2$, and (b) 1-nm F$_8$ZnPc/ML-WS$_2$ collected at different times (shown in the legend) after the He-lamp (used for the UPS measurement) was turned on. For the ML-WS$_2$, the spectrum gradually shifts to the left when the sample is continuously illuminated by the UV light source, which shows that the sample is gradually charged up. This observation typically indicates that the sample has a relatively poor conductivity. As a result, net charges generated from the photoemission process slowly builds up on the sample surface. The sample shows much less charging after the F$_8$ZnPc is deposited. Compared to the ML-WS$_2$, the heterostructure can have improved photoconductivity because long-lived carriers are generated from charge separation.